Nanostructured Y 2 O 3 ceramics elaborated by Spark Plasma Sintering of nanopowder synthesized by PEG assisted combustion method: The influence of precursor morphological characteristics

Radenka Krsmanović Whiffen, Damien Bregiroux, Bruno Viana

Nanostructured Y_2O_3 ceramics elaborated by Spark Plasma Sintering of nanopowder synthesized by PEG assisted combustion method: the influence of precursor morphological characteristics

Radenka M. Krsmanović Whiffen[a, c], Damien Bregiroux[b,]*, Bruno Viana[c]

[a] Vinča Institute of Nuclear Sciences, University of Belgrade, P.O. Box 522, 11001 Belgrade, Serbia

[b] Sorbonne Universités, UPMC Univ Paris 06, CNRS, Collège de France, Laboratoire de Chimie de la Matière Condensée de Paris, 4 place Jussieu, 75005 Paris, France

[c] Institut de Recherche de Chimie Paris (IRCP), CNRS – Chimie Paris Tech – Paris Sciences et Lettres PSL UMR8247, 11 rue Pierre et Marie Curie, 75005 Paris, France

* Corresponding author. Tel.: + 331 442 756 79

E-mail address: damien.bregiroux@upmc.fr (D. Bregiroux)

Abstract

Dense yttria ceramics were prepared by Spark Plasma Sintering of a nanopowder synthesized using a PEG assisted combustion method. Densification occurs between 800°C and 900°C without any additive. This corresponds to one of the lowest sintering temperature found in the literature for Y_2O_3. Because of a significant release of organic species, the Y_2O_3 precursors obtained by this synthesis route contains macropores that have a negative impact on the final microstructure. We show that the emergence of these macropores can be minimized by decreasing the annealing temperature used for the precursor powder (in a temperature range of 300°C - 650°C) as opposed to the usual

800°C. Finally, a precursor annealed at 650°C allows us to obtain fully dense ceramics, with a very fine and homogeneous microstructure (and a grain size around 300 nm). Vickers microhardness and fracture toughness were measured and discussed in relation to the microstructure of the ceramics.

Keywords

A. Grain growth; Sintering

B. Electron microscopy

D. Y_2O_3

Highlights

- Full densification at very low temperature (a very reactive Y_2O_3 nanopowder)
- Ceramics of fine grain size (around 300 nm) with good mechanical properties
- Agglomerated starting nanopowders lead to opaque ceramics

1. Introduction

Yttria, Y_2O_3, is a cubic structure bixbyite oxide and a very promising material for optical devices and high temperature refractories due to its wide optical transmission range (0.2–8 μm), high corrosion resistivity, thermal stability, and its high melting point of around 2430 °C [1]. For optical applications, yttria is preferably fabricated in the form of transparent ceramic as, due to its refractory characteristics, it is hard to obtain single crystals [2]. Although the first transparent yttria ceramic was reported almost 50 years ago [3] it has attracted and continues to attract numerous researchers, who explore the various means of its production. The opportunity to create such optically transparent

ceramics relies on the control of two key parameters: residual porosity (10^{-2} to 10^{-3} vol. % or less) and grain boundaries purity. For these reasons the sintering of polycrystalline ceramics for optical applications typically involves long treatments at high temperatures (usually 70–80 % of the melting point) generally using hot pressing (HP) [4], hot-isostatic pressing (HIP) [5-7], or vacuum sintering [8,9], with the aim of obtaining a very dense final bulk material. Nevertheless, yttria ceramics prepared in this way generally have large grains, in the range of hundreds of microns, leading to low mechanical strength which in turn limits opportunities for their practical application. In recent years, the idea of making nanostructured ceramics, *i.e.* ceramics with sub-micron sized grains, starting from appropriate ultrafine precursor nanopowders, has been of interest to numerous researchers. The main strategy is to modify standard fabrication methods and to study the effects of starting powder characteristics on the sintering and microstructure of the ceramics [10-13]. The main benefit of using nanostructured ceramics lies in the fact that their mechanical properties, such as hardness and fracture toughness, are generally improved when grain size is maintained at a nanometric scale [14]. The requirement of achieving almost total densification with an extremely small grain size has led towards the use of non-conventional sintering methods, generally combining low sintering temperatures and high pressures. The Spark Plasma Sintering (SPS) method is one of the most commonly investigated method so far [15-23]. In parallel, many efforts have been made over recent decades in terms of the development of new synthesis routes for Y_2O_3 nanopowders in order to obtain a powder with better sintering behaviour [24-25]. In our previous studies of bixbyite oxides in the form of highly crystalline nanopowders we proposed and used extensively a polyethylene glycol (PEG) – assisted combustion method known as the polymer

complex solution (PCS) [26-28]. The simple equipment required and low energy consumption levels makes this method attractive for the fabrication of diverse oxide nanomaterials with excellent qualities for ceramic fabrication [29-30] including the potential extension of this approach to industrial scale production. The goal of this work was to evaluate the Spark Plasma Sintering behaviour of Y_2O_3 nanopowders synthesized using a PEG assisted combustion method. This work was performed with a focus on the influence of precursor agglomeration and nanoparticles size that are directly related to the temperature used in the post-synthesis thermal treatment of the Y_2O_3 nanopowders. Densification and final microstructure were examined in relation to the synthesis and sintering conditions. The obtained results were compared with those found in the literature. Conclusions were drawn concerning the potential use of the PEG assisted combustion method for the elaboration of Y_2O_3 ceramics for possible optical and mechanical applications.

2. Experimental

Several tens of grams of Y_2O_3 nanopowder were synthesized using the PCS method [26-28]. Aqueous solutions of stoichiometric quantities of yttrium nitrate were prepared by dissolving appropriate quantities of Y_2O_3 (Alfa Aesar, 99.9%) in a hot nitric acid solution. All the chemicals were of the highest purity available and were used without further purification.

In the prepared solutions, PEG 200 (Alfa Aesar) was added in a 1:1 mass ratio to the oxide used. After stirring for several hours at 80°C, this metal-PEG solution transformed into a metal-PEG resin-like solid complex that was further combusted at 800°C in air, and then annealed at 800°C in air for 2 hours, resulting in a fine, white-

coloured powder (sample 800°C-2h) . This powder was used for the first part of our experiment. For comparison, sintering tests were also performed on commercial Y_2O_3 powder (Alfa Aesar). For the second part of our experiment, where we wanted to explore the influence of different nanoparticle size and powder agglomeration, a new batch of Y_2O_3 powders was produced at lower annealing temperatures. We decided to change the end part of the PCS procedure by decreasing both the temperature used for combustion and for the final calcination. For the new batch of Y_2O_3 nanopowders, the metal- PEG complex was combusted at only 350°C in air, and then calcinated at 300°C for 2 hours, resulting in a fine black powder. With further calcination at temperatures lower than 800°C (400, 500, 550, and 650) for 2 hours we were able to tune the crystallinity and particle size of Y_2O_3 nanopowder and get a white powder. One sample was annealed for 10 hours at 450°C.

The X-ray diffraction measurements of the Y_2O_3 nanopowder were obtained at room temperature on a Philips PW 1050 instrument, using Ni filtered Cu $K\alpha_{1,2}$ radiation (λ = 1.5418 Å), in a 2θ range from 10° to 120° (with a step size of 0.02° and a counting time of 12 s per step). The X-ray diffraction measurements of the second set of powders, with additional thermal treatments, were obtained at room temperature, on a Bruker D8, using Ni filtered Cu $K\alpha_{1,2}$ radiation (λ = 1.5418 Å), in a 2θ range from 15° to 70°.

Thermal stability and possible phase transitions were studied using a Setaram DTA-TG instrument. The Y_2O_3 gel sample (i.e. the metal-PEG resin-like solid complex), with a mass of 32.8 mg, was put into a Pt crucible, heated up to 800°C and then cooled under an argon atmosphere at a rate of 5 °C min^{-1}. The specific surface area of the ground powders was measured according to the BET method, using N_2 as an adsorbate (Bellsorp, Bell, Japan). The samples were degassed for 12 hours at 150°C prior to the

analysis. The microstructure of the Y_2O_3 nanopowders, subjected to different thermal treatments, was analyzed by transmission electron microscopy (TEM FEI G2 operating at 120 kV) in bright field. For the TEM observations, a suspension of particles in ethanol was ultrasonicated for 20 minutes and dropped onto a holey carbon copper grid. Sintering experiments were performed under a 0.1 mbar vacuum using the SPS technique (Dr. Sinter 515S Syntex machine). The Y_2O_3 powder was filled into a graphite die with an inner diameter of 8 mm. Approximately 0.25 grams of the precursor powder was needed for a ceramic disc of a thickness of 2 mm. The temperature was monitored by a thermocouple, ranging from room temperature to the sintering temperature. Sample shrinkage was followed by the displacement of the lower punch. The heating rate and cooling rate were set to 100 °C.min^{-1} and 50 °C.min^{-1}, respectively. Pressure was applied gradually from room temperature to 400 °C and maintained at its maximum value until the beginning of the cooling step. The pressure was then removed over the course of 10 minutes. The sintered sample was then annealed under flowing air at 700 °C for 10 hours in order to remove carbon contamination from the graphite die and the oxygen vacancies generated by the reducing environment during sintering.

The microstructures of the ceramic samples were observed on fractures using a SEM (Hitachi S-3400N), working at an accelerating voltage of 20 kV. The surface of the samples was coated with a thin layer of carbon prior to observation. The relative density of the SPS sintered discs was measured by the Archimedes method in distilled water, assuming that the theoretical density of Y_2O_3 was 5.03 g cm^{-3} [31]. Vickers microhardness and fracture toughness were measured on polished ceramics using a

microhardness tester (Bruck MHT 200). Microhardness *Hv* was determined using the following equation:

$$H_v = k\left(\frac{P}{d^2}\right) \quad (1)$$

where *P* is the applied load (500g, *i.e.* 4.903 N), *k* the shape factor (0.1891) and *d* the indent diagonal (mm).

The fracture toughness was calculated using the following equation [32]:

$$K_{IC} = 0.016\left(\frac{E}{H_v}\right)^{\frac{1}{2}}\left(\frac{P}{C^{\frac{3}{2}}}\right) \quad (2)$$

where *E* is the Young's modulus of Y_2O_3 (179.8 GPa, according to [33]) and *C* the linear size of the radial crack.

All the final results represent the average of 20 indentation tests.

3. Results and discussion

3.1. Precursors and Y_2O_3 powders characterization

Figure 1 shows the morphology of the two yttria powders with which we started this study. The commercial Y_2O_3 powder (Figure 1 a and b) consists of well crystallized particles (confirmed by XRD) with a diameter in the range of 50 – 100 nm. Those particles are strongly agglomerated to form hard and dense agglomerates of 1 – 4 μm in size. The resulting specific surface area of this powder is indeed very low (around 1.1 $m^2.g^{-1}$).

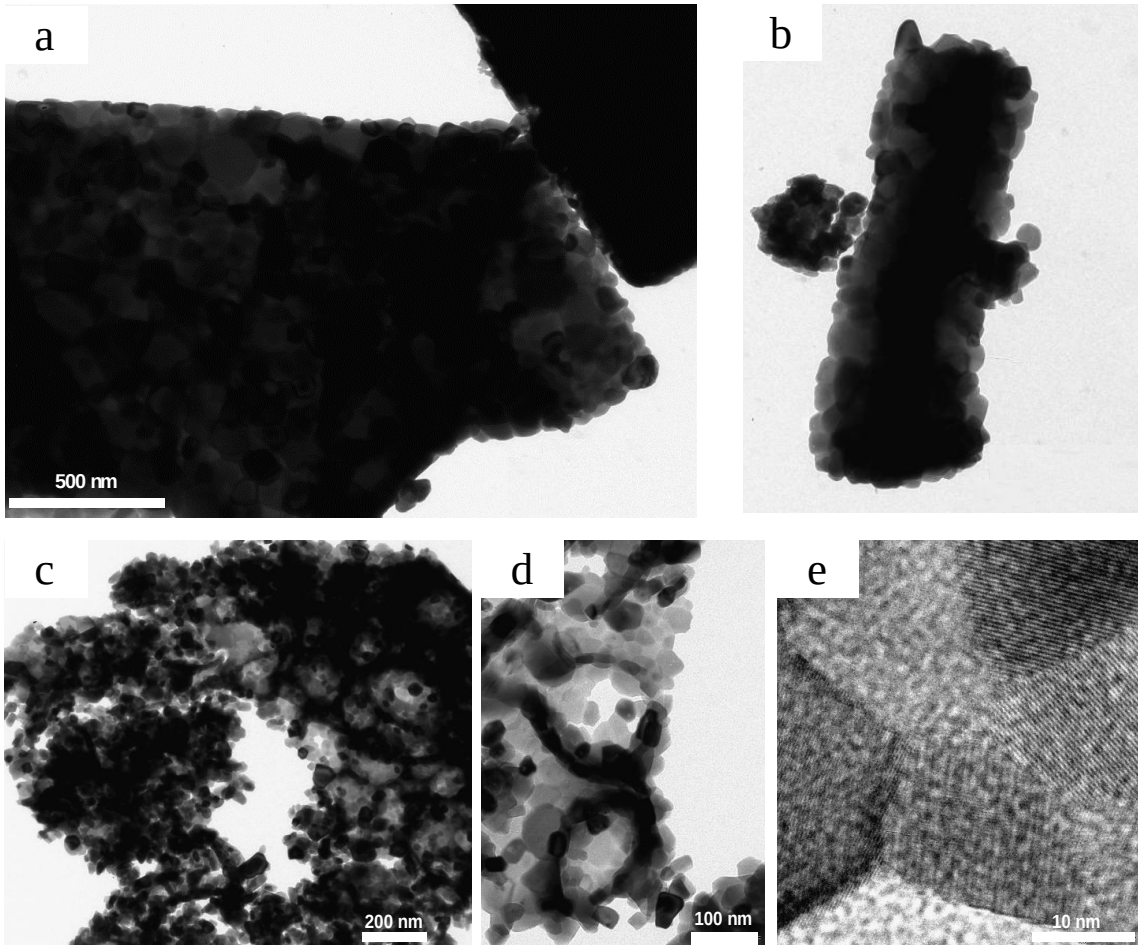

Figure 1. Morphology of the commercial (a and b) and PCS-produced (PEG Mw = 200) (c, d and e) yttria powder used in this study.

The synthesized Y_2O_3 powder exhibits a very different morphology. It consists of well crystallized nanoparticles, clearly visible in Figure 1 (c, d and e), with an average diameter of 20 – 30 nm. Those particles form loose agglomerates, 1 – 2 μm in size, containing holes which are 50 – 300 nm in diameter. The thermal behaviour of the metal-PEG complex (the Y_2O_3 gel sample) under heating, up to 800°C, and the ideal temperature for its decomposition were determined by TG/DTA analysis (see Figure 2). Most of the weight loss, around 65% of the initial weight, occurs between 100°C and 450°C. This corresponds to water evaporation and the decomposition of all organic

species. A slight weight loss also occurs at around 600°C. This is probably due to the decomposition of yttrium carbonate [30]. We noticed that the powders from the second batch, when calcinated at temperatures below 500 °C are either black or grey, and become white when calcinated beyond this temperature.

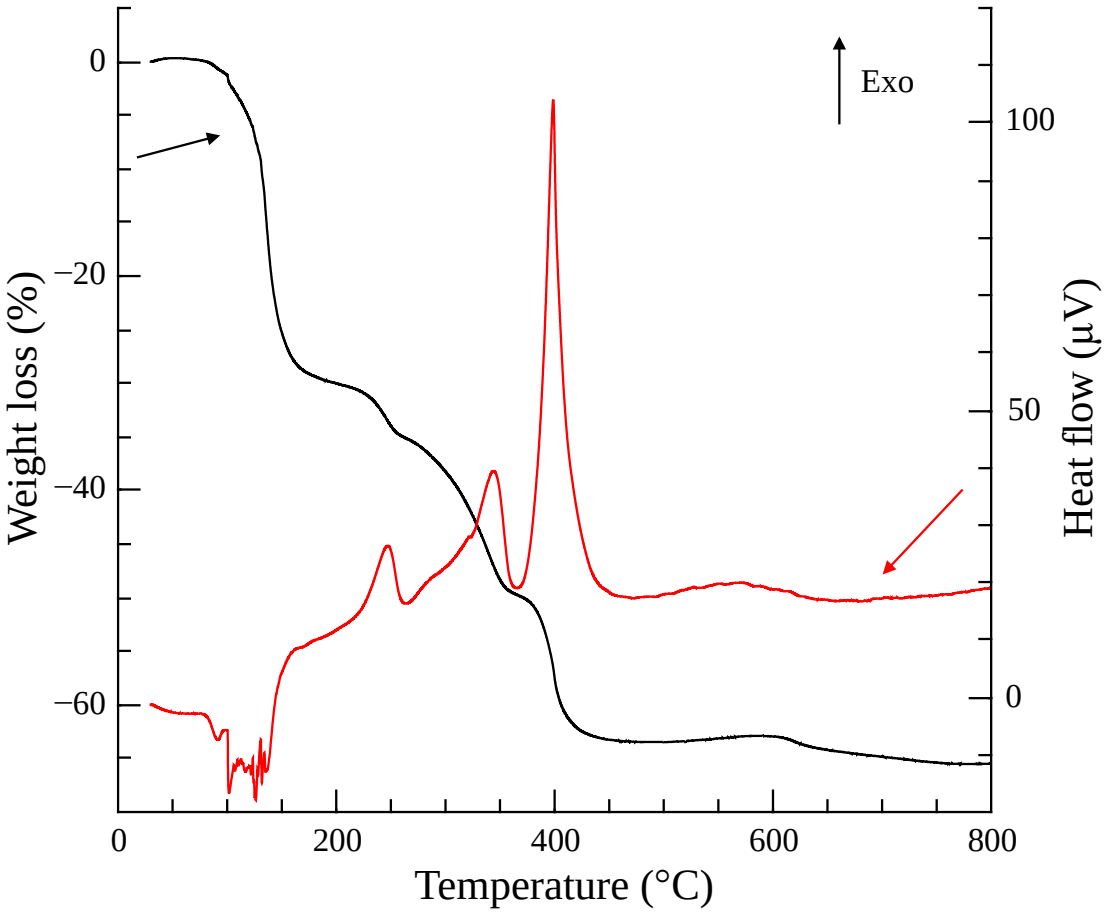

Figure 2. Thermal behaviour of the metal-PEG resin-like solid complex (the Y_2O_3 gel sample).

The specific surface area (SSA) of lab-synthesized Y_2O_3 is much higher than that of the commercial powder and is in the range of 22 to 25 $m^2.g^{-1}$ depending on the post-synthesis thermal treatments: the starting powder (*i.e.* the one annealed at 300°C)

exhibited a specific surface area of 25.4 $m^2.g^{-1}$. As expected, the specific surface area decreases with the increase in the annealing temperature from 300 to 800°C (25 $m^2.g^{-1}$ for 400°C, 24.8 $m^2.g^{-1}$ for 500°C and 550°C, and 21.8 $m^2.g^{-1}$ for 800°C; see Figure 3), with a transient increase at 650°C (25.6 $m^2.g^{-1}$) due to the decomposition of the carbonate species (see the TG plot in Figure 2). The sample annealed at 800°C was the one produced using the standard PCS procedure (from the first batch).

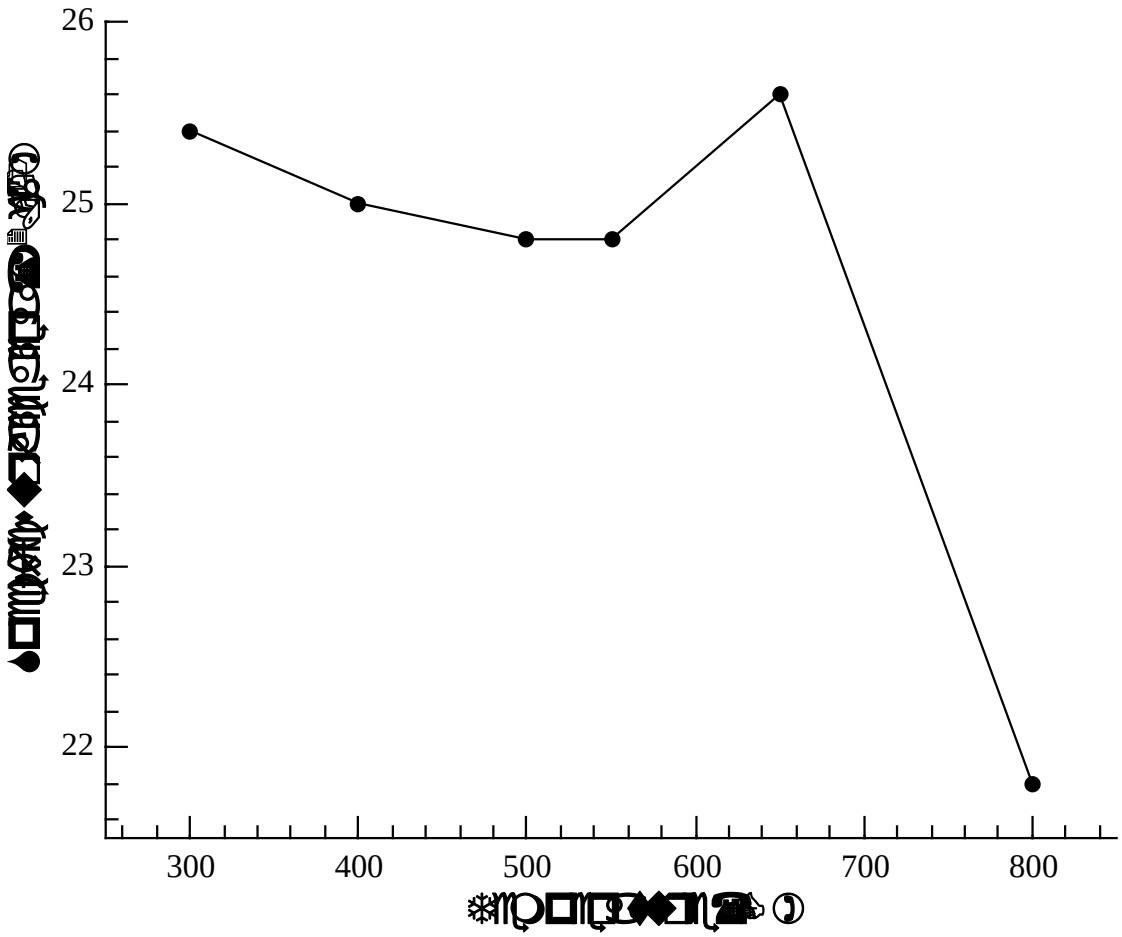

Figure 3. Specific surface area of the raw Y_2O_3 powders after annealing at different temperatures and the PCS-standardly produced sample annealed at 800 °C.

XRD analyses revealed that the cubic form of Y_2O_3 (SG *Ia*-3 n° 206, *a* = 10.6023 Å) can be observed in the samples annealed at 300°C and above (see Figure 4). The XRD peaks are broad and weak for sample annealed at 300°C and progressively become sharper and more intense as both the temperature and annealing time increase. This can be directly associated with the increase in nanoparticle size, as can be observed in Figure 5. For sample annealed at 400°C, the nanoparticle size is found to be as small as 6 nm. The particle size starts to increase rapidly when the annealing temperature is greater than 650°C. For the 800°C treatment, the nanoparticles have an average size of around 25 nm.

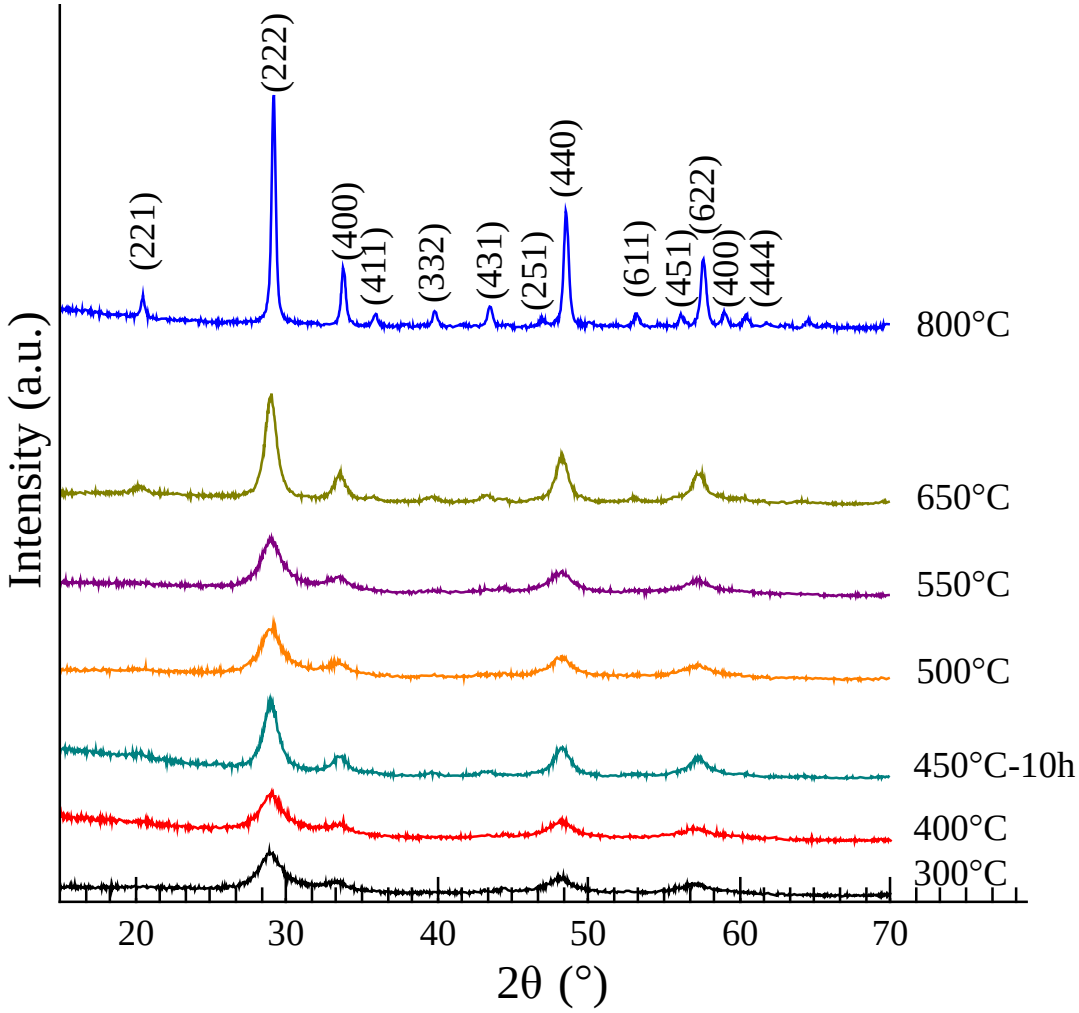

Figure 4. XRD patterns of the raw powders after different thermal treatment temperatures *vs.* the PCS-standard sample annealed at 800 °C.

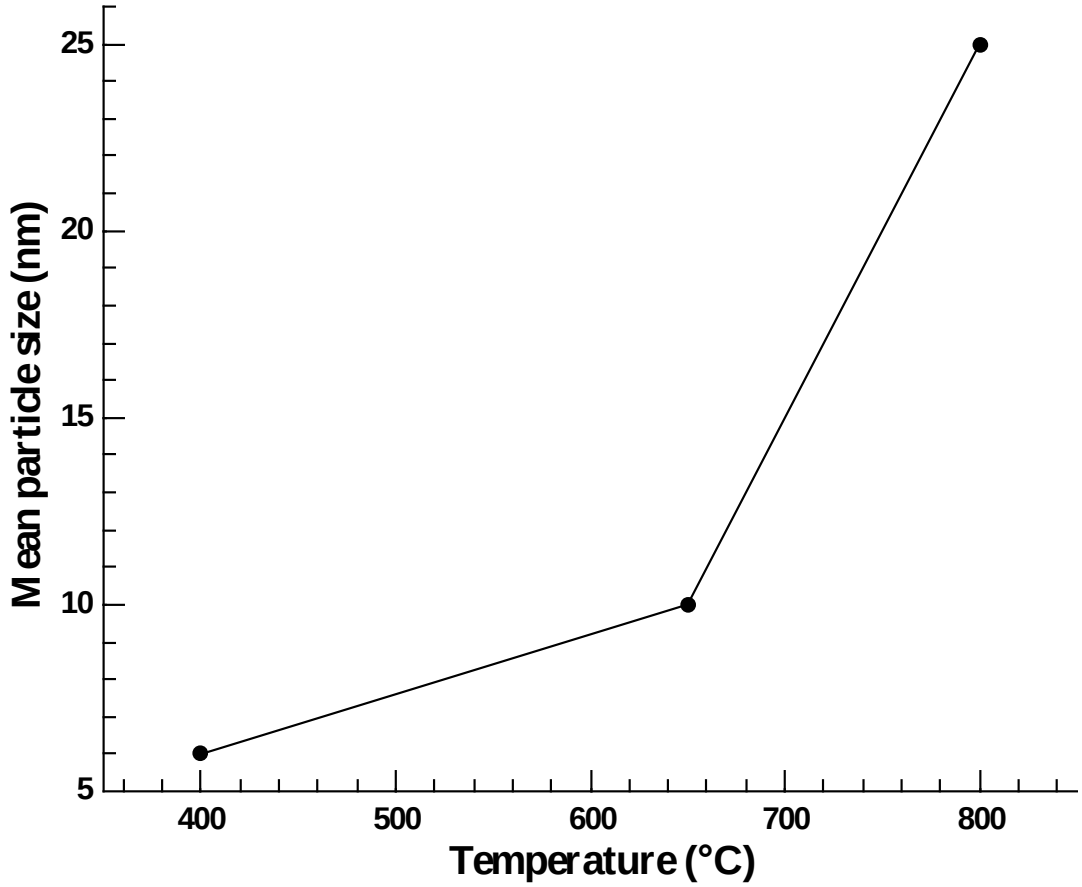

Figure 5. Mean nanoparticle size as a function of the annealing temperature, as estimated from TEM pictures.

Examples of different powder morphologies are shown in Figure 6. We can clearly see that macroporosity is present in the samples annealed at 400°C and at higher temperatures, due to the elimination of organic species during annealing. No conditions have so far been found for the PCS production of nanopowders without such

macroporosity. The size of the macropores is the same regardless of the annealing temperature; however the nanoparticles seems to have weaker grain boundaries when the annealing is performed at a lower temperature. We expected that for the studied conditions, the macropores (in the range of 20-200 nm) could be broken more easily when pressure was applied during Spark Plasma Sintering.

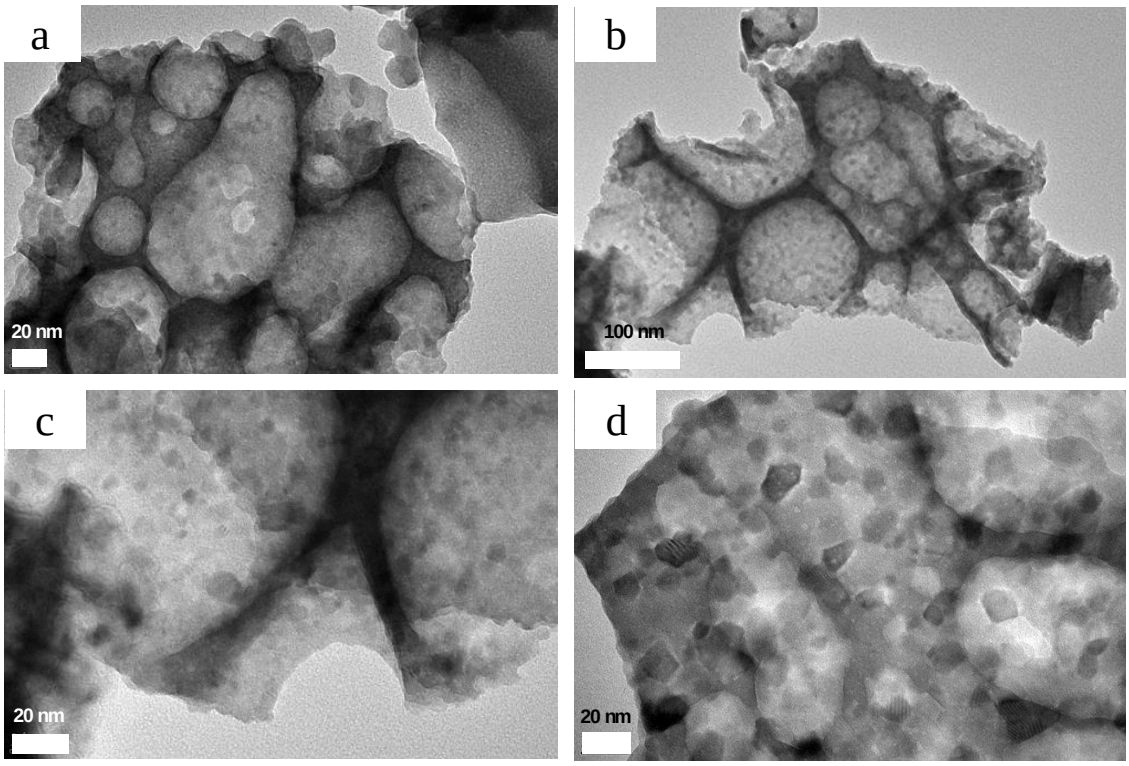

Figure 6. TEM pictures of Y_2O_3 powders after annealing at 400°C (a), 450°C-10 hours (b and c) and 650°C (d).

3.2. Spark Plasma Sintering and the characterization of ceramic samples

The synthesized powders were sintered by using the Spark Plasma Sintering technique. Figure 7 depicts the densification behaviour of the Y_2O_3 nanopowder, PCS- synthesized

at 800°C, when sintered under a uniaxial pressure of 50 MPa and 100 MPa. Linear shrinkage, plotted in Figure 7 in arbitrary units, includes the Thermal Expansion contribution of the graphite tool. For this reason, we removed the scale, since punch displacement also depends on the amount of powder and the extent of its pre-compaction.

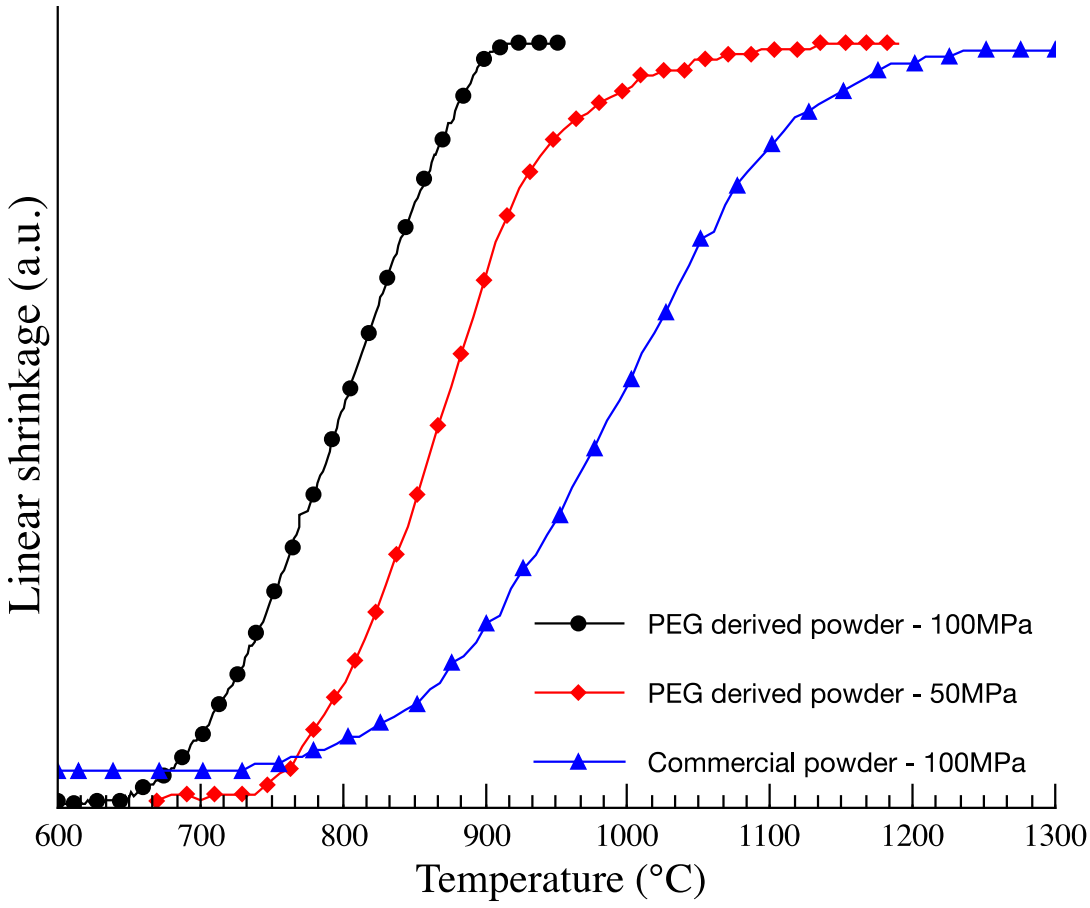

Figure 7. SPS linear shrinkage for the PEG derived Y_2O_3 samples sintered under 50 MPa (red lozenges) and 100 MPa (black circles) uniaxial pressures and the commercial powder sintered under 100 MPa (blue triangles).

Sintering under 100 MPa instead of 50 MPa lowers the densification temperature by 80°C. In addition, at high temperatures, the end of the densification curve is sharper for sintering under 100 MPa. Irom *et al.* recently found that applying high pressure during Spark Plasma Sintering led to a finer microstructure and consequently increased levels of hardness and fracture toughness [35]. As a result, all the subsequent SPS experiments were performed under a uniaxial pressure of 100 MPa.

Our results highlighted that, for PEG-derived powder, under an applied pressure of 100 MPa, shrinkage begins at around 650°C and ends at 900°C, which is similar to the lowest sintering temperature found in the literature for the Spark Plasma Sintering of undoped Y_2O_3 [15,21,22,36]. For comparison, the experimental curve obtained from the commercial powder under an applied pressure of 100 MPa is presented, showing that shrinkage starts at 725°C and is completed only at 1250°C. Moreover, the densification process is much faster for the PEG derived powder, since the temperature range for densification is only 250°C (as opposed to 525°C for the commercial powder).

The final relative density of the produced ceramic discs was around 98% for the PEG derived powder (at a sintering temperature of 1000°C), and 99% for the commercial one (at a sintering temperature of 1300°C). Despite very good densification behaviour, the ceramic samples made from the PEG derived powder were all opaque even when the sintering temperature was set to higher values (with tests performed up to 1500°C). By contrast, the ceramics made from commercial powder were very slightly translucent when produced at a sintering temperature of 1300°C or higher.

Figure 8 shows the mean grain size evolution, from 200 nm to 3 µm, with the respective sintering temperature increase from 1000°C to 1550°C, for the PEG derived powder synthesized at 800°C. For each of the samples, the relative density is greater than 98%

of the theoretical density. Grain growth is negligible below 1200°C, so that fully dense Y_2O_3 ceramics can be obtained with a mean grain size of as low as 210 nm at 1000°C. For the commercial Y_2O_3 powder used in this study the required sintering temperature was at least 1300°C, and it was not possible, to obtain ceramics with a mean grain size below 1 μm.

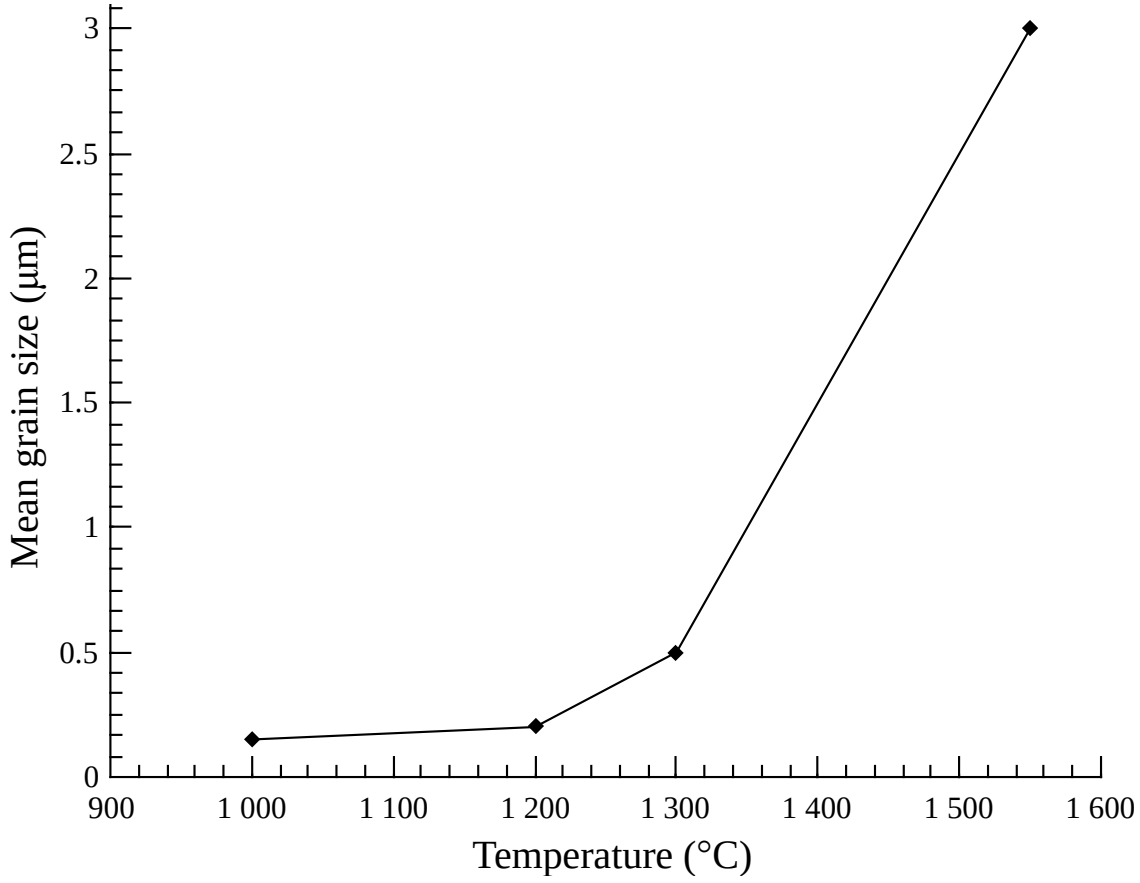

Figure 8. Mean grain size *vs.* sintering temperature for the ceramic samples made from PEG derived powder synthesized at 800°C (dwell time: 1min, uniaxial pressure: 100 MPa).

Figure 9 shows the typical microstructure obtained after Spark Plasma Sintering of the standard PEG derived Y_2O_3 nanopowder. The grain size distribution is homogeneous. We also observed the presence of some residual porosity with a size in the range of 100 – 400 nm. This porosity is responsible for the opacity of all the ceramics samples, even those with a very high relative density. The size of those pores is equivalent to the macropore values observed in the starting nanopowders (see Figure 1). This suggests that the opacity observed for all the ceramic samples stems from the macroporosity formed during the calcination step of the precursor nanopowders. As previously discussed, we expected that the macropores would be broken more easily during Spark Plasma Sintering once the powder was annealed at a lower temperature. Thus we annealed PEG derived Y_2O_3 powder at temperatures lower than 800 °C and selected two powders for further Spark Plasma Sintering tests: one annealed at 450°C for 10 hours (sample 450°C-10h) and the other annealed at 650°C for 1h (sample 650°C-1h). The obtained results are presented in Figure 10. Note that in this graph, the shrinkage observed below 400°C is mainly due to the application of uniaxial pressure. Beyond this temperature, the pressure is maintained at 100 MPa.

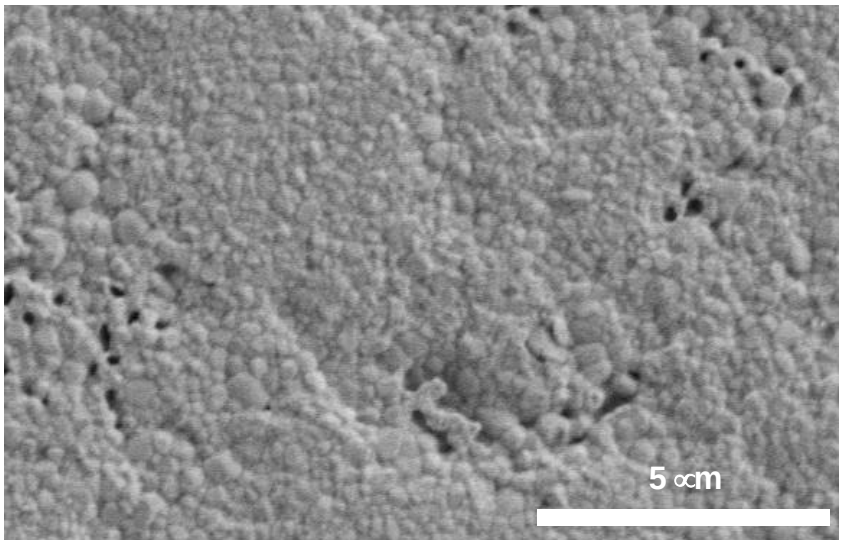

Figure 9. Microstructure of Y_2O_3 ceramics sintered by SPS at 1000°C-1min under 100 MPa uniaxial pressure from PEG-derived powder annealed at 800°C.

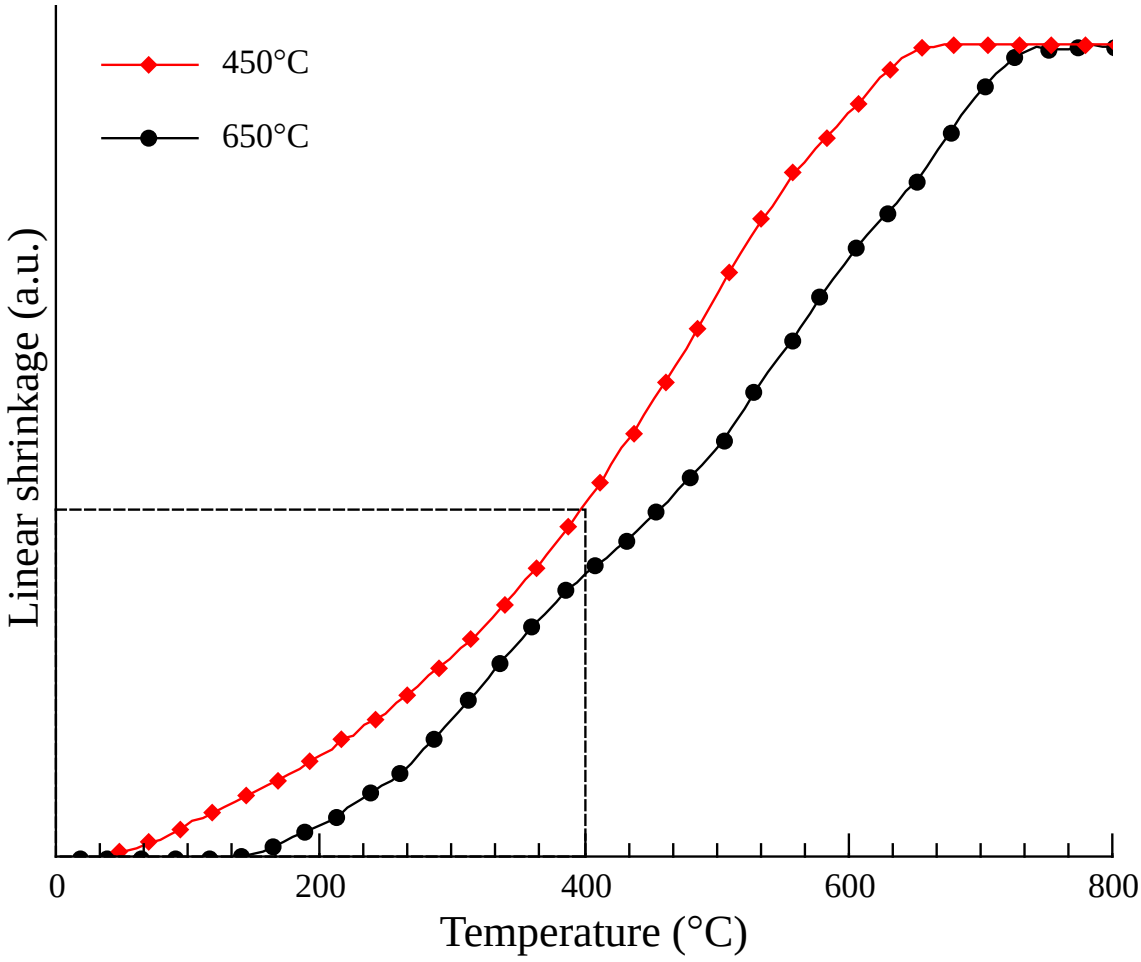

Figure 10. SPS linear shrinkage under 100 MPa uniaxial pressure for samples made of PEG derived powder annealed at 450°C–10h (red lozenges) and 650°C (black circles).

As expected, the temperature of densification decreases as the annealing temperature of the powder decreases. Thus, the densification of the ceramic sample prepared from the powder annealed at 450°C-10h is completed at 650°C, while this process is prolonged to about 750°C for the other sample (see Figure 10). Nevertheless, the maximum

relative density of the ceramic obtained from the 450°C-10h powder after sintering at 1000°C is 95.5%, whereas a ceramic sample with a relative density of 100 % is obtained under the same SPS conditions for the 650°C-1h powder.

Figure 11 shows the typical microstructures obtained after Spark Plasma Sintering at 1000°C of the powders previously annealed at 450°C-10h and 650°C-1h. The mean grain sizes are around 250 nm and 300 nm, respectively. The ceramic sample made from the powder annealed at 450°C-10h exhibits residual porosity, unlike the other ceramic sample (650°C-1h) which appears to be fully dense. The lower relative density of the first sample is probably due to the release of the carbonate species for the powder annealed at 450°C (see Figures 2 and 3). Since the sample made from the powder annealed at 650°C is free of carbonate species, no porosity is formed around 650°C during the sintering step. Note that this sample is very slightly translucent, by contrast with the one obtained from the powder annealed at 450°C-10h (Figure 12). It is worth noting that in those two samples, unlike in the ceramics made from the powder annealed at 800°C, no macropores could be observed in the microstructures, demonstrating that reducing the annealing temperature of the Y_2O_3 precursor is actually a good way of avoiding the emergence of macropores. However, the process optimization of different steps of the ceramic fabrication (for example green body shaping and thermal profile during SPS sintering and the subsequent annealing step) is needed in order to achieve better optical characteristics in the studied ceramic samples.

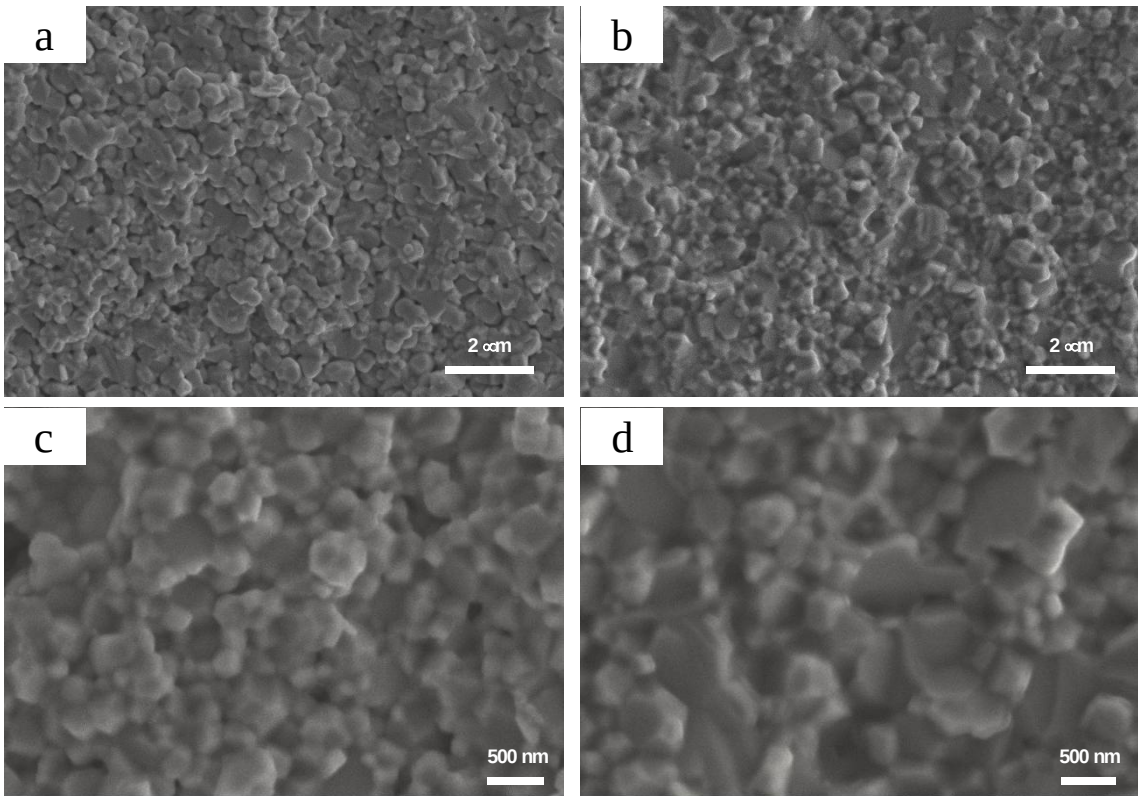

Figure 11. Typical microstructures of Y_2O_3 ceramics sintered at 1000°C from the PEG-derived powder annealed at 450°C for 10 hours (a and c) and 650°C for 2 hours (b and d).

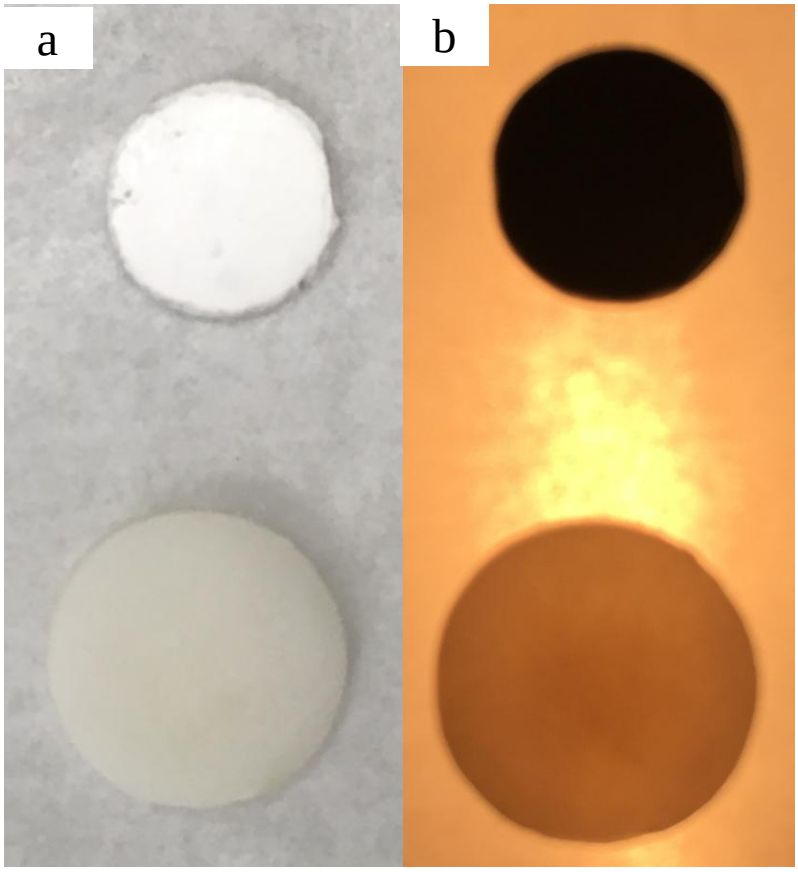

Figure 12. Ceramics made from the powder annealed at 450°C-10h (upper) and 650°C-1h (lower) placed on a light source, switched OFF (a) and ON (b).

Vickers microhardness and fracture toughness were measured on three Y_2O_3 ceramic samples, all sintered at 1000°C for 1 min: one made from the raw commercial powder, one made from the powder annealed at 650°C-1h, and one made from the powder annealed at 450°C-10h. The results are summarized in Table 1.

Table 1. Vickers hardness (Hv), fracture toughness (K_{IC}), relative density and mean grain size for selected Y_2O_3 ceramics samples.

Sample	Hv (GPa)	K_{IC} (MPa.m$^{1/2}$)	Relative density (%)	Mean grain size (μm)

Y_2O_3 commercial	6.8 +/- 0.1	0.67 +/- 0.03	99.0	1-3
Y_2O_3 annealed at 650°C-1h	8.2 +/- 0.1	0.90 +/- 0.1	100	0.3
Y_2O_3 annealed at 450°C-10h	4.0 +/- 0.1	ND	95.5	0.25

The values of microhardness and fracture toughness are consistent with those found in the literature [37,38]. As previously shown, the sample made from the powder annealed at 450°C-10h contains a substantial number of residual pores (see Figure 11a). Consequently, the microhardness value is low and the fracture toughness is impossible to measure to an acceptable accuracy. A typical indent with radial cracks is shown in Figure 13. It is worth noting that the indent diagonal is in the range 25 - 40 μm, *i.e.* more than 30 times longer than the mean grain diameter. This means that grain boundaries have a strong effect on the value of microhardness and fracture toughness, since grain boundaries stop the propagation of the dislocations and microcracks induced by the application of the indenter on the surface [39]. As expected, for dense samples, microhardness and fracture toughness increase as grain size decreases (see Table 1). According to the literature, the microhardness and fracture toughness of Y_2O_3 ceramics can be further improved through sintering additives, such as La_2O_3 or ZrO_2 [38,40].

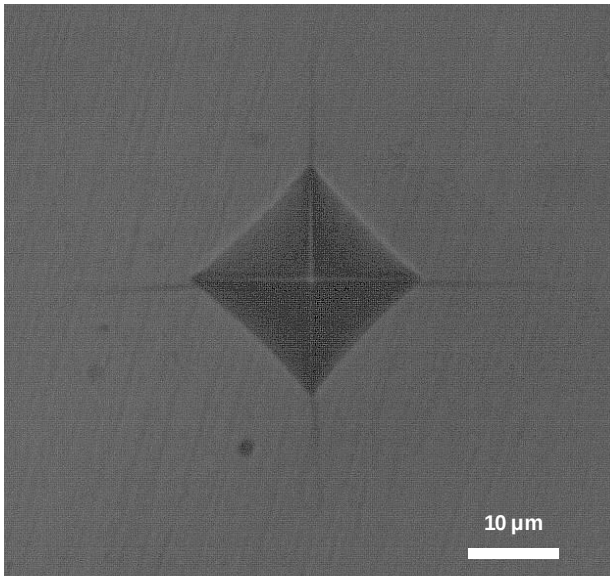

Figure 13. Optical micrograph of the indent in the sample made from the commercial Y_2O_3 and sintered by SPS at 1300°C-1min.

4. Conclusions

The polyethylene glycol (PEG) – assisted combustion method known as the polymer complex solution (PCS) is a simple synthesis route that leads to a very reactive Y_2O_3 nanopowder which can be densified using the Spark Plasma Sintering technique between 800°C and 900°C without any additive. This corresponds to one of the lowest sintering temperatures found in the literature for Y_2O_3 ceramics.

Because of a significant release of organic species during synthesis and post-synthesis thermal treatments, Y_2O_3 precursors obtained by the PCS route contain macropores that have a negative impact on the final microstructure (meaning the presence of residual porosity in the ceramic samples). Our results show that these macropores can be minimized by decreasing the combusted and annealing temperature of the precursor. Nevertheless, a minimum temperature of 650°C is required in order to fully eliminate the carbonate species. Finally, a precursor annealed at 650°C allows us to obtain a fully

dense ceramic, with a very fine and homogeneous microstructure (and an average grain size of around 300 nm). Vickers microhardness and fracture toughness values were found to be close to the values reported in the literature for undoped Y_2O_3 ceramics. Because of the very good sinterability, the ceramic made from the PCS nanopowder annealed at 650°C had a much smaller grain size and thus better mechanical properties (a hardness of approximately 8.2 GPa and an appropriate fracture toughness of 0.9 MPa m ½) than the ceramics made from the micron-sized commercial Y_2O_3 powder (a hardness of approximately 6.8 GPa and a fracture toughness of 0.67 MPa m ½). We are hopeful that the further optimization of the different steps in the ceramic fabrication process (*i.e.* the shaping and subsequent Spark Plasma Sintering steps) will lead to fully dense nanostructured ceramic materials with better optical and even better mechanical properties, without the need for additives during sintering. In addition, given that precursor morphological characteristics can be tailored by changing the temperature needed to start the combustion process and for annealing, we believe that the findings presented in this paper will be of use to many fellow researchers working on materials produced by combustion synthesis or modifications of that process.

Acknowledgments

The authors are grateful to the trainee Johann Merlet for his enthusiastic participation in the sintering experiments and Isabelle Genois for SEM and TEM observations at the LCMCP laboratory. They also acknowledge Dr. Philippe Vermaut for indentation experiments at Chimie ParisTech and Dr. Željka Antić from the Vinca Institute of Nuclear Sciences for providing the standard PCS-produced Y_2O_3 powder (800°C) and its gel sample. R.K.W. acknowledges La Mairie de Paris for the award of a ”Research in

Paris" 2013–2014 fellowship, which enabled her stay at Chimie Paris Tech for the realization of this research.

References

[1] L.B. Kong, Y.Z. Huang, W.X. Que, T.S. Zhang, S. Li, J. Zhang, Z.L. Dong, D.Y. Tang, Transparent Ceramics, XII, Springer International Publishing AG, 2015.

[2] A. Fukabori, T. Yanagida, J. Pejchal, S. Maeo, Y. Yokota, A. Yoshikawa, T. Ikegami, F. Moretti, K. Kamada, Optical and scintillation characteristics of Y_2O_3 transparent ceramic. J. Appl. Phys. 107 (2010) 073501.

[3] R.A. Lefever, J. Matsko, Transparent yttrium oxide ceramics, Mater. Res. Bull. 2 (1967) 865–869.

[4] S.R. Podowitz, R. Gaume, R.S. Feigelson, Effect of europium concentration on densification of transparent Eu:Y_2O_3 scintillator ceramics using hot pressing, J. Am. Ceram. Soc. 93 (2010) 82–88.

[5] H. Eilers, Fabrication, optical transmittance, and hardness of IR-transparent ceramics made from nanophase yttria. J. Eur. Ceram. Soc. 27 (2007) 4711–4717.

[6] J. Mouzon, A. Maitre, L. Frisk, N. Lehto, M. Odén, Fabrication of transparent yttria by HIP and the glass-encapsulation method, J. Eur. Ceram. Soc. 29 (2009) 311–316.

[7] H. Mingsheng, L. Jianbao, L. Hong, G. Gangfeng, L. Long, Fabrication of transparent polycrystalline yttria ceramics by combination of SPS and HIP, J. Rare Earths 24 (2006) 222–224.

[8] Y.H. Huang, D.L. Jiang, J.X. Zhang, Q.L. Lin, Fabrication of transparent lanthanum-doped yttria ceramics by combination of two-step sintering and vacuum sintering, J. Am. Ceram. Soc. 92 (2009) 2883–2887.

[9] L.L. Jin, G.H. Zhou, S. Shimai, J. Zhang, S.W. Wang, ZrO_2-doped Y_2O_3 transparent ceramics via slip casting and vacuum sintering, J. Eur. Ceram. Soc. 30 (2010) 2139–2143.

[10] J.R. Groza, Nanosintering, Nanostructured Mater. 12 (1999) 987–992.

[11] J.P. Kelly, O.A. Graeve, Effect of powder characteristics on nanosintering, in: R.H.R. Castro, K. van Benthem (Eds.), Sintering, Springer-Verlag, Berlin Heidelberg, 2013, pp. 57–95.

[12] I.W. Chen, X.H. Wang, Sintering dense nanocrystalline ceramics without final-stage grain growth, Nature 404 (2000) 168–171.

[13] M.A.A. Attia, R. Orrù, F. Delogu, S. Montinaro, S. Garroni, E.M.M. Ewais, G. Cao, Effects of prior annealing on the spark plasma sintering of nanostructured Y_2O_3 powders, J. Am. Ceram. Soc. 98 (2015) 1453–1459.

[14] O. Tokariev, L. Schnetter, T. Beck, J. Malzbender, Grain size effect on the mechanical properties of transparent spinel ceramics, J. Eur. Ceram. Soc. 33 (2013) 749-757.

[15] R. Chaim, R. Marder, C. Estournes, Optically transparent ceramics by spark plasma sintering of oxide nanoparticles, Scripta Mater. 63 (2010) 211–214.

[16] R. Chaim, A. Shlayer, C. Estournes, Densification of nanocrystalline Y2O3 ceramic powder by spark plasma sintering, J. Eur. Ceram. Soc. 29 (2009) 91–98.

[17] Y. Futami, T. Yanagida, Y. Fujimoto, J. Pejchal, M. Sugiyama, S. Kurosawa, Y. Yokota, A. Ito, A. Yoshikawa, T. Goto, Optical and scintillation properties of Sc_2O_3, Y_2O_3 and Lu_2O_3 transparent ceramics synthesized by SPS method, Radiat. Meas. 55 (2013) 136-140.

[18] R. Chaim, R. Marder, C. Estournés, Z. Shen, Densification and preservation of ceramic nanocrystalline character by spark plasma sintering, Adv. Appl. Ceram. 111 (2012) 280–285.

[19] J. Liu, Z. Shen, M. Nygren, B. Su, T.W. Button, Spark plasma sintering behavior of nano-sized (Ba,Sr)TiO_3 powders: determination of sintering parameters yielding nanostructured ceramics, J. Am. Ceram. Soc. 9 (2006) 2689–2694.

[20] M. Eriksson, Y. Liu, J. Hu, L. Gao, M. Nygren, Z. Shen, Transparent hydroxyapatite ceramics with nanograin structure prepared by high pressure spark plasma sintering at the minimized sintering temperature, J. Eur. Ceram. Soc. 31 (2011) 1533–1540.

[21] H. Yoshida, K. Morita, B.N. Kim, K. Hiraga, M. Kodo, K. Soga, T. Yamamoto, Densification of nanocrystalline yttria by low temperature spark plasma sintering, J. Am. Ceram. Soc. 91 (2008) 1707–1710.

[22] L. An, A. Ito, T. Goto, Transparent yttria produced by spark plasma sintering at moderate temperature and pressure profiles, J. Eur. Ceram. Soc. 32 (2012) 1035–1040.

[23] N. Poirot, D. Bregiroux, P. Boy, C. Autret-Lambert, P. Belleville, L. Bianchi, Sintering of nanostructured Sc_2O_3 ceramics from sol-gel-derived nanoparticles, Ceram. Int. 41 (2015) 3879–3887.

[24] M. Hajizadeh-Oghaz, R. Shoja Razavi, M. Bareka, M. Naderi, S. Malekzadeh, M. Rezazadeh, Synthesis and characterization of Y_2O_3 nanoparticles by sol-gel process for transparent ceramics applications, J. Sol-Gel Sci. Technol. 78 (2016) 682–691.

[25] M. Khajelakzay, R.S. Razavi, M. Barekat, M. Naderi, Synthesis of Yttria Nanopowders by Two Precipitation Methods and Investigation of Synthesis Conditions, Int. J. Appl. Ceram. Technol. 13 (2016) 209–218.

[26] R. Krsmanović, Ž. Antić, B. Bártová, M.D. Dramićanin, Characterization of rare-earth doped Lu_2O_3 nanopowders prepared with polymer complex solution synthesis, J. Alloys Compd. 505 (2010) 224–228.

[27] Ž. Antić, R. Krsmanović, M. Wojtowicz, E. Zych, B. Bártová, M.D. Dramićanin, Preparation, structural and spectroscopic studies of $(Y_xLu_{1-x})_2O_3:Eu^{3+}$ nanopowders, Opt. Mater. 32 (2010) 1612–1617.

[28] R.M. Krsmanović, Ž. Antić, M.G. Nikolić, M. Mitrić, M.D. Dramićanin, Preparation of $Y_2O_3:Eu^{3+}$ nanopowders via polymer complex solution method and luminescence properties of the sintered ceramics, Ceram. Int. 37 (2011) 525–531.

[29] R.M. Krsmanović, Ž. Antić, B. Bártová, M.G. Brik, M.D. Dramićanin, Fabrication of polycrystalline $(Y_{0.7}Gd_{0.3})_2O_3:Eu^{3+}$ ceramics: the influence of initial pressure and sintering temperature on its morphology and photoluminescence activity, Ceram. Int. 38 (2012) 1303–1313.

[30] R. Krsmanović Whiffen, Ž. Antić, B. Milićević, M. Pošarac-Marković, Dj. Janaćković, M. D. Dramićanin, M. G. Brik, I. Steins, Dj. Veljović, Polycrystalline $(Y_{0.7}Gd_{0.3})_2O_3:Eu^{3+}$ ceramics fabricated by spark plasma sintering: Densification and microstructure development, Ceram. Int. 40 (2014) 8853–8862.

[31] L. Smrcok, Rietveld Refinement of Y_2O_3 using the Pearson VII Profile Shape Function, Crystal Res. Tech. 24 (1989) 607–611.

[32] G.R. Anstis, P. Chantikul, B.R. Lawn, D.B. Marshall, A critical-evaluation of indentation techniques for measuring fracture toughness. 1. Direct cracks measurements, J. Am. Ceram. Soc. 64 (1981) 533–538.

[33] O. Yeheskel, O. Tevet, Elastic moduli of transparent yttria, J. Am. Ceram. Soc. 82 (1999) 136–144.

[34] J.M. Luiz, J.R. Matos, I. Giolito, M. Ionashiro, Thermal behaviour of the basic carbonates of lanthanum- europium, Thermochim. Acta 254 (1995) 209–218.

[35] E. Irom, M. Zakeri, A.S. Ahangari, H. Zadeh, S. Safian, A. Rahbari, Low-pressure fabrication of IR-transparent Y_2O_3 via spark plasma sintering, Micro Nano Lett. 11 (2016) 688–691.

[36] H. Zhang, B.N. Kim, K. Morita, Y. Hidehiro, K. Hiraga, Y. Sakka, Fabrication of transparent yttria by high-pressure spark plasma sintering, J. Am. Ceram. Soc. 94 (2011) 3206–3210.

[37] K. Serivalsatit, B. Kokuoz, B. Yazgan-Kokuoz, M. Kennedy, J. Ballato, Synthesis, processing, and properties of submicrometer-grained highly transparent yttria ceramics, J. Am. Ceram. Soc. 93 (2010) 1320–1325.

[38] K. Ning, J. Wang, D. Luo, J. Ma, J. Zhang, Z.L. Dong, L.B. Kong, D. Y. Tang, Fabrication and characterization of highly transparent Yb^{3+}:Y_2O_3 ceramics, Opt. Mater. 50 (2015) 21–24.

[39] I.J. McColm, Ceramic Hardness, Plenum Press, New York, 1990.

[40] L. Zhang, J. Feng, W. Pan, Vacuum sintering of transparent Cr:Y_2O_3 ceramics, Ceram. Int. 41 (2015) 8755–8760.